Supplementary Materials for "Sensing the spin of an individual Ce adatom"

Markus Ternes,[1,2*] Christopher P. Lutz,[3] Andreas J. Heinrich,[4,5] Wolf-Dieter Schneider,[6,7]

[1]RWTH Aachen University, Institute of Physics, D-52074 Aachen, Germany
[2]Peter-Grünberg-Institute, Forschungszentrum Jülich, D-52425 Jülich, Germany
[3]IBM Almaden Research Center, San Jose, California 95120, USA
[4]Center for Quantum Nanoscience, Institute for Basic Science (IBS), Seoul 03760, Republic of Korea
[5]Physics Department, Ewha Womans University, Seoul, Republic of Korea
[6]Ecole Polytechnique Fédérale de Lausanne (EPFL), Institut de Physique, CH-1015 Lausanne, Switzerland
[7]Fritz-Haber-Institute of the Max-Planck-Society, Faradayweg 4-6, D-14195 Berlin, Germany

[*]Corresponding author. e-mail: ternes@physik.rwth-aachen.de

Determination of the adsorption sites

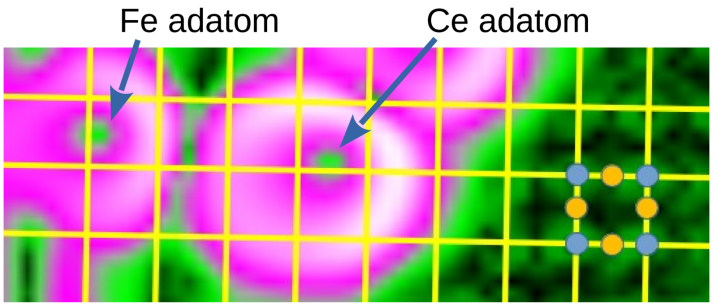

Figure S1: **Determination of the adsorption sites of Fe and Ce adatoms.** False-color curvature image of a constant current STM topography ($V = 10$ mV, $I = 1$ nA) revealing atomic resolution of the Cu_2N substrate as well as the position of Fe and Ce-adatoms. Yellow lines mark the atomic rows of the substrate. Yellow and blue circles mark the position of surface Cu and N atoms, respectively.

Spectra of a Ce adatom close to the rim of a Cu_2N path

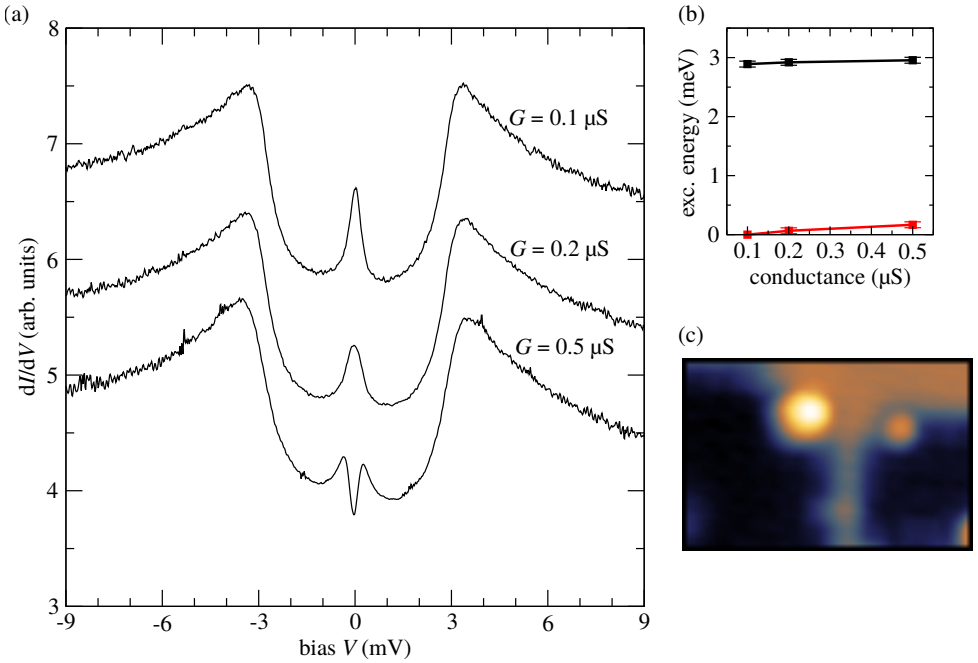

Figure S2: **Spectra of a Ce adatom close to the rim of a Cu_2N path showing only weak splitting when probed with the functionalized tip** (a) Differential conductance, dI/dV, spectra measured at different set-point conductances, $G = I/V$, on top of a Ce adatom close to the rim of a Cu_2N patch. The curves a shifted vertically for better visualization. (b) Extracted transition energies. (c) Constant current topography of the Ce adatom (bright spot). Note that the smaller spots with similar topographic height as the bare Cu(100) substrate are individual missing N defects of the Cu_2N. ($V = 10$ mV, $I = 1$ nA, size: 3.8×2.5 nm^2)

rr

Residual error of the least square fit shown in Fig. 2a

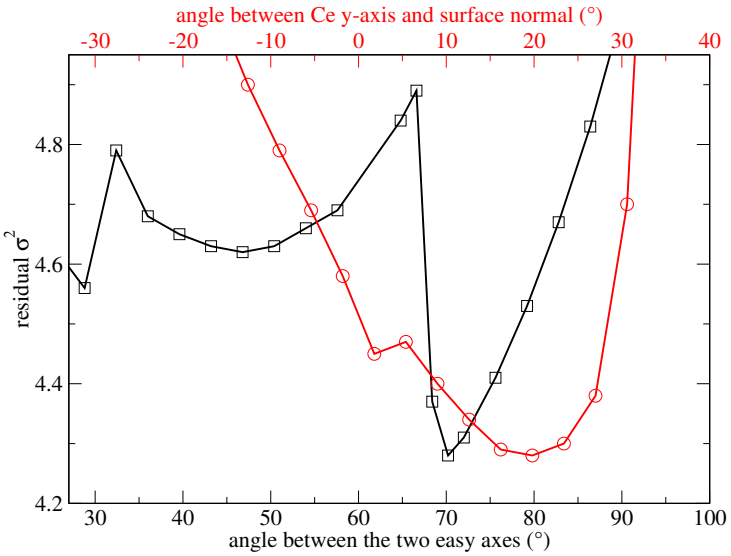

Figure S3: **Residual error of the least square fit shown in Fig. 2a.** Plot of the sum of the least squares determined between the simulation and the experimental data displayed in Figure 2a of the main text in dependence of the two fit angles (red and black symbols). Except for an overall scaling and a conductance offset, all parameters as the magnetic aniosotropies and coupling parameters are fixed and determined independently by the spectroscopic data of the individual spin systems on tip and sample (Fig. 1d and 1f of the main text). Fixing one angle at its optimum we vary the corresponding other. The fit error becomes minimal for $\approx 70°$ between the two easy axes of the spin systems and an angle of $\approx 18°$ between the surface normal and the y-axis of the Ce cluster on the tip apex. Full lines are guides to the eyes.

Spin Hamiltonian and perturbative transport model

The spin Hamiltonian

We model the electron transport between tip and sample by allowing both electrodes to contain a spin system. This results in the following total Hamiltonian:

$$\hat{H} = \hat{H}^{\mathrm{s}}_{\mathrm{bath}} + \hat{H}^{\mathrm{t}}_{\mathrm{bath}} + \hat{H}^{\mathrm{s}}_{\mathrm{imp}} + \hat{H}^{\mathrm{t}}_{\mathrm{imp}} + \hat{H}_{\mathrm{imp-imp}} + \hat{H}\text{'}. \tag{S1}$$

Here, the Hamiltonians $\hat{H}^{\mathrm{s}}_{\mathrm{bath}}$ and $\hat{H}^{\mathrm{t}}_{\mathrm{bath}}$ describe the two electrodes of tip and sample, $\hat{H}^{\mathrm{s}}_{\mathrm{imp}}$ and $\hat{H}^{\mathrm{t}}_{\mathrm{imp}}$ the two impurity spins on tip and sample, $\hat{H}_{\mathrm{imp-imp}}$ the interaction between the two spins, and $\hat{H}$' the transport of electrons between the electrodes.

We assume that the electrodes are large bathes with a flat and featureless density of electron states allowing us to describe them in second quantization as:

$$\hat{H}^{\mathrm{s}}_{\mathrm{bath}} + \hat{H}^{\mathrm{t}}_{\mathrm{bath}} = \sum_{\substack{j=\mathrm{s,\,t}\\k,\sigma}} \epsilon_{jk\sigma} \hat{a}^{\dagger}_{jk\sigma} \hat{a}_{jk\sigma}, \tag{S2}$$

with $\hat{a}^{\dagger}_{jk\sigma}$ ($\hat{a}_{jk\sigma}$) as the creation (annihilation) operators for electrons at the electrode $j = \mathrm{s}$ (sample) and $j = \mathrm{t}$ (tip) with momentum k, spin σ, and the energy $\epsilon_{jk\sigma}$. In the small energy range of our interest around the Fermi energy, we describe the reservoirs with energy independent spin density matrices $\varrho_{\mathrm{s,\,t}} = |\phi\rangle\langle\phi| = \frac{1}{2}(\hat{\sigma}_0 + \vec{n}_{\mathrm{s,\,t}} \cdot \hat{\boldsymbol{\sigma}})$. Here, the spin-polarization of the electrons is accounted for by the direction and amplitude of the vector $\vec{n}_{\mathrm{s,\,t}}$, with $\hat{\boldsymbol{\sigma}} = (\hat{\sigma}_x, \hat{\sigma}_y, \hat{\sigma}_z)$ as the standard Pauli matrices, and $\hat{\sigma}_0$ as the (2×2) identity matrix. With this convention, the spin polarization is identical to the relative imbalance between majority and minority spin densities, $\eta_{\mathrm{s,\,t}} = |\vec{n}_{\mathrm{s,\,t}}| = \left|\frac{\rho_\uparrow - \rho_\downarrow}{\rho_\uparrow + \rho_\downarrow}\right|$, where $\uparrow$ and $\downarrow$ account for the two different spin directions along the quantization axis.

To model the spin-states at the sample and tip impurity we utilize effective Hamiltonians which include axial (D) and transverse magnetic anisotropy (E) [33]:

$$\begin{aligned}
\hat{H}^{\mathrm{s}}_{\mathrm{imp}} &= D_{\mathrm{s}}(\hat{S}^{\mathrm{s}}_z)^2 + E_{\mathrm{s}}\left((\hat{S}^{\mathrm{s}}_x)^2 - (\hat{S}^{\mathrm{s}}_y)^2\right),\\
\hat{H}^{\mathrm{t}}_{\mathrm{imp}} &= D_{\mathrm{t}}(\hat{S}^{\mathrm{t}'}_z)^2 + E_{\mathrm{t}}\left((\hat{S}^{\mathrm{t}'}_x)^2 - (\hat{S}^{\mathrm{t}'}_y)^2\right),
\end{aligned} \tag{S3}$$

with $\hat{\mathbf{S}} = (\hat{S}_x, \hat{S}_y, \hat{S}_z)$ as the generalized spin operators of the tip or sample impurity. In this Hamiltonian each impurity has its magnetically hard ($D > 0$) or easy ($D < 0$) axis pointing along the z-direction. For any $E \neq 0$ the remaining two orthogonal axes are further distinguished with the y-direction as the magnetically intermediate axis.

In general, the two spin impurities at the tip apex and on the sample do not share the same coordinate system. Therefore, we use a set of Euler angles α, β, γ to rotate the axes of the

spin-system at the tip apex with respect to the usually better known anisotropy axes of the spin system at the surface:

$$\hat{S}_i^{\mathrm{t}'} = \hat{R}_z(\gamma)\hat{R}_y(\beta)\hat{R}_x(\alpha)\,\hat{S}_i^{\mathrm{t}}\,\hat{R}_x^{\dagger}(\alpha)\hat{R}_y^{\dagger}(\beta)\hat{R}_z^{\dagger}(\gamma) \quad \forall i \in \{x,y,z\}, \tag{S4}$$

with the rotation operators $\hat{R}_x(\alpha) = \exp(-i\alpha\hat{S}_x^{\mathrm{t}})$, $\hat{R}_y(\beta) = \exp(-i\beta\hat{S}_y^{\mathrm{t}})$, and $\hat{R}_z(\gamma) = \exp(-i\gamma\hat{S}_z^{\mathrm{t}})$.

The interaction Hamiltonian $\hat{H}_{\mathrm{imp-imp}}$ between the two spin impurities can be written as:

$$\hat{H}_{\mathrm{imp-imp}} = \hat{\mathbf{S}}^{\mathrm{s}}\mathbf{J}\hat{\mathbf{S}}^{\mathrm{t}}, \tag{S5}$$

with $\mathbf{J}$ as the interaction tensor of rank two. Because we found only highly symmetric interactions, we simplify equation S5 to a Heisenberg-like interaction, $J\hat{\mathbf{S}}^{\mathrm{s}} \cdot \hat{\mathbf{S}}^{\mathrm{t}}$, or even further to an Ising-like interaction, which we can also describe as an external magnetic field B_z^{eff} induced by the dark spin on the surface acting on the spin states of the tip:

$$\hat{H}_{\mathrm{imp-imp}} = J_z\hat{S}_z^{\mathrm{s}} \cdot \hat{S}_z^{\mathrm{t}} = -g\mu_B B_z^{\mathrm{eff}} \cdot \hat{S}_z^{\mathrm{t}}. \tag{S6}$$

To calculate the flow of tunneling current between tip and sample, we treat $\hat{H}$' in equation S1 as a perturbation, which enables the transport of electrons via Kondo-like spin-flip or potential scattering processes on the impurities in first and second order Born approximation [15–27, 34, 35] Such a model has previously been used successfully on different quantum spin systems [28–31, 44, 46, 47]

Perturbative transport model with one active spin

First, we will discuss only one spectroscopically active spin on one electrode as used in the simulations for the figures 1d, 1f, and 3 of the main paper.

This leads to the following transport Hamiltonian $\hat{H}$':

$$\hat{H}' = \hat{V}_{\mathrm{t}\to\mathrm{s}} + \hat{V}_{\mathrm{s}\to\mathrm{t}} + \hat{V}_{\mathrm{t}\to\mathrm{t}} \tag{S7}$$

$$\hat{V}_{\mathrm{t}\to\mathrm{s}} = \sum_{\substack{\sigma,\sigma'\\k,k'}} T_0\,\hat{a}_{\mathrm{s}k'\sigma'}^{\dagger}\,\hat{a}_{\mathrm{t}k\sigma}\left(\frac{1}{2}\hat{\boldsymbol{\sigma}}\cdot\hat{\mathbf{S}}^{\mathrm{t}} + U^{\mathrm{t}}\hat{\sigma}_0\cdot\hat{1}\right), \tag{S8}$$

$$\hat{V}_{\mathrm{s}\to\mathrm{t}} = \sum_{\substack{\sigma,\sigma'\\k,k'}} T_0\,\hat{a}_{\mathrm{t}k'\sigma'}^{\dagger}\,\hat{a}_{\mathrm{s}k\sigma}\left(\frac{1}{2}\hat{\boldsymbol{\sigma}}\cdot\hat{\mathbf{S}}^{\mathrm{t}} + U^{\mathrm{t}}\hat{\sigma}_0\cdot\hat{1}\right), \tag{S9}$$

$$\hat{V}_{\mathrm{t}\to\mathrm{t}} = \frac{1}{2}\sum_{\substack{\sigma,\sigma'\\k,k'}} J^{\mathrm{t}}\,\hat{a}_{\mathrm{t}k'\sigma'}^{\dagger}\,\hat{a}_{\mathrm{t}k\sigma}\hat{\boldsymbol{\sigma}}\cdot\hat{\mathbf{S}}^{\mathrm{t}}, \tag{S10}$$

where we set, without loss of generality, the active spin on the tip as needed to describe the Ce-cluster attached to the tip apex. Note that reducing the transport to one spectroscopically

active spin does not necessarily mean a reduction of the Hamiltonian (S1) to one impurity. The passive, dark spin influences via the interaction Hamiltonian $\hat{H}_{\mathrm{imp-imp}}$ the spectrum.

The coupling T_0 between tip and sample is adjusted to match the set point counductance $G = I/V$ of the experiment, J is the coupling between the spin and its hosting electrode whereby $|J| \gg |T_0|$, and U is the Coulomb scattering parameter.

In this model, the transition probability $W_{i\to f}^{j\to j'}$ for an electron to tunnel from electrode j to electrode j' and concomitantly change the state of the spin on the tip apex from its initial (i) to its final (f) state with the corresponding energies ε_i and ε_f evaluated up to second order Born approximation is:

$$W_{i\to f}^{j\to j'} \propto \left(|M_{i\to f}|^2 + \rho_0 J \sum_m \left(\frac{M_{i\to m} M_{m\to f} M_{f\to i}}{\varepsilon_i - \varepsilon_m} + \text{c. c.} \right) \right) \delta(\varepsilon_i - \varepsilon_f). \tag{S11}$$

Because we treat the tunneling only as a small perturbation, we can separate the full Hilbert-space into sub-spaces which contain the states of reservoir electrons $|\phi\rangle$ and the states of the spin system $|\Psi\rangle$. This allows us to calculate the transition matrix elements as [34]

$$M_{i\to f} = \sum_{i',f'} \sqrt{\lambda_{i'}\lambda_{f'}} \, \langle \phi_{f'}, \Psi_f | \left(\frac{1}{2} \hat{\boldsymbol{\sigma}} \cdot \hat{\boldsymbol{S}} + U \hat{\sigma}_0 \hat{1} \right) | \phi_{i'}, \Psi_i \rangle \,, \tag{S12}$$

with $|\phi_{i'}, \Psi_i\rangle = |\phi_{i'}\rangle \, |\Psi_i\rangle$ as product states and $|\phi_{i'}\rangle$ as the eigenstates and $\lambda_{i'}$ as the eigenvalues of the density matrices $\varrho_{i'}$ of the electron reservoirs participating in the scattering process.

Note that the combination of equation S3 and S6 leads to the Hamiltonian as written in equation 1 of the main text, that neglecting any spin polarization in equation S12 leads to equation 2 of the main text, and that we neglect in our approach any additional electron transport between tip and sample which does not involve spin-flip or potential scattering processes described by the equations S8 and S9.

With equation S11 we can now continue to calculate the transition rates between the initial $|\Psi_i\rangle$ and final $|\Psi_f\rangle$ eigenstates of the impurities sub-Hamiltonian $\hat{H}_{\mathrm{imp}}^{\mathrm{s}} + \hat{H}_{\mathrm{imp}}^{\mathrm{t}} + \hat{H}_{\mathrm{imp-imp}}$ using Fermi's golden rule:

$$\begin{aligned} \Gamma_{i\to f}^{\mathrm{t}\to\mathrm{s}}(eV) &\propto \int_{-\infty}^{\infty} d\epsilon \, W_{i\to f}^{\mathrm{t}\to\mathrm{s}} f(\epsilon - eV, T_{\text{eff}})[1 - f(\epsilon - \epsilon_f + \epsilon_i, T_{\text{eff}})], \\ \Gamma_{i\to f}^{\mathrm{s}\to\mathrm{t}}(eV) &\propto \int_{-\infty}^{\infty} d\epsilon \, W_{i\to f}^{\mathrm{s}\to\mathrm{t}} f(\epsilon + eV, T_{\text{eff}})[1 - f(\epsilon - \epsilon_f + \epsilon_i, T_{\text{eff}})], \end{aligned} \tag{S13}$$

with $f(\epsilon, T)$ as the Fermi-Dirac distribution and $T_{\text{eff}} \approx 1$ K as the effective temperature in the experiment.

Because we found that spin-pumping and out-of equilibrium effects [31, 49] do not play a significant role in the experiments discussed here, we assume steady-state occupation which follows the Boltzmann distribution $p_i(T_{\text{eff}}) = Z^{-1} \exp(-\frac{\varepsilon_i}{k_B T_{\text{eff}}})$ with Z as the canonical partition

function. Now we can continue to calculate the tunneling current to:

$$I(eV) = e\sum_{i,j} p_i \left(\Gamma^{\mathrm{t}\to\mathrm{s}}_{i\to f}(eV) - \Gamma^{\mathrm{s}\to\mathrm{t}}_{i\to f}(eV)\right), \tag{S14}$$

and by numerical differentiation $\mathrm{d}I/\mathrm{d}V$ and $\mathrm{d}^2I/\mathrm{d}V^2$.

Perturbative transport model with two active spins

Interestingly, the transition matrix elements for scattering between tip and sample changes significantly when we include a second spin so that both electrodes, tip and sample, have an active spin system through which the electron transport has to occur. The transport Hamiltonian $\hat{H}$' changes into:

$$\hat{H}' = \hat{V}_{\mathrm{s}\to\mathrm{t}} + \hat{V}_{\mathrm{t}\to\mathrm{s}} + \hat{V}_{\mathrm{s}\to\mathrm{s}} + \hat{V}_{\mathrm{t}\to\mathrm{t}} \tag{S15}$$

$$\begin{aligned}\hat{V}_{\mathrm{t}\to\mathrm{s}} = \sum_{\substack{\sigma,\sigma'\\k,k'}} T_0\, \hat{a}^\dagger_{\mathrm{s}k'\sigma'}\, \hat{a}_{\mathrm{t}k\sigma} \Bigg[&\left(\frac{1}{2}\hat{\boldsymbol{\sigma}}\cdot(\hat{\mathbf{S}}^{\mathrm{t}}\otimes\hat{1}^{\mathrm{s}}) + U^{\mathrm{t}}\hat{\sigma}_0\cdot\hat{1}^{\mathrm{ts}}\right)\left(\frac{1}{2}\hat{\boldsymbol{\sigma}}\cdot(\hat{1}^{\mathrm{t}}\otimes\hat{\mathbf{S}}^{\mathrm{s}}) + U^{\mathrm{s}}\hat{\sigma}_0\cdot\hat{1}^{\mathrm{ts}}\right)\\ &+ \left(\frac{1}{2}\hat{\boldsymbol{\sigma}}\cdot(\hat{1}^{\mathrm{t}}\otimes\hat{\mathbf{S}}^{\mathrm{s}}) + U^{\mathrm{s}}\hat{\sigma}_0\cdot\hat{1}^{\mathrm{ts}}\right)\left(\frac{1}{2}\hat{\boldsymbol{\sigma}}\cdot(\hat{\mathbf{S}}^{\mathrm{t}}\otimes\hat{1}^{\mathrm{s}}) + U^{\mathrm{t}}\hat{\sigma}_0\cdot\hat{1}^{\mathrm{ts}}\right)\Bigg],\end{aligned} \tag{S16}$$

$$\begin{aligned}\hat{V}_{\mathrm{s}\to\mathrm{t}} = \sum_{\substack{\sigma,\sigma'\\k,k'}} T_0\, \hat{a}^\dagger_{\mathrm{t}k'\sigma'}\, \hat{a}_{\mathrm{s}k\sigma} \Bigg[&\left(\frac{1}{2}\hat{\boldsymbol{\sigma}}\cdot(\hat{1}^{\mathrm{t}}\otimes\hat{\mathbf{S}}^{\mathrm{s}}) + U^{\mathrm{s}}\hat{\sigma}_0\cdot\hat{1}^{\mathrm{ts}}\right)\left(\frac{1}{2}\hat{\boldsymbol{\sigma}}\cdot(\hat{\mathbf{S}}^{\mathrm{t}}\otimes\hat{1}^{\mathrm{s}}) + U^{\mathrm{t}}\hat{\sigma}_0\cdot\hat{1}^{\mathrm{ts}}\right)\\ &+ \left(\frac{1}{2}\hat{\boldsymbol{\sigma}}\cdot(\hat{\mathbf{S}}^{\mathrm{t}}\otimes\hat{1}^{\mathrm{s}}) + U^{\mathrm{t}}\hat{\sigma}_0\cdot\hat{1}^{\mathrm{ts}}\right)\left(\frac{1}{2}\hat{\boldsymbol{\sigma}}\cdot(\hat{1}^{\mathrm{t}}\otimes\hat{\mathbf{S}}^{\mathrm{s}}) + U^{\mathrm{s}}\hat{\sigma}_0\cdot\hat{1}^{\mathrm{ts}}\right)\Bigg],\end{aligned} \tag{S17}$$

$$\hat{V}_{\mathrm{s}\to\mathrm{s}} = \frac{1}{2}\sum_{\substack{\sigma,\sigma'\\k,k'}} J^{\mathrm{s}}\, \hat{a}^\dagger_{\mathrm{s}k'\sigma'}\, \hat{a}_{\mathrm{s}k\sigma}\hat{\boldsymbol{\sigma}}\cdot(\hat{1}^{\mathrm{t}}\otimes\hat{\mathbf{S}}^{\mathrm{s}}), \tag{S18}$$

$$\hat{V}_{\mathrm{t}\to\mathrm{t}} = \frac{1}{2}\sum_{\substack{\sigma,\sigma'\\k,k'}} J^{\mathrm{t}}\, \hat{a}^\dagger_{\mathrm{t}k'\sigma'}\, \hat{a}_{\mathrm{t}k\sigma}\hat{\boldsymbol{\sigma}}\cdot(\hat{\mathbf{S}}^{\mathrm{t}}\otimes\hat{1}^{\mathrm{s}}). \tag{S19}$$

It might surprise that equations S16 and S17 contain not only one term but also a term in reverse scattering order. The consideration of both terms is necessary because we do not have any information of the scattering order. Expanding the important parts of the brackets leads to

the following terms:

$$
\begin{aligned}
&\left(\frac{1}{2}\hat{\boldsymbol{\sigma}}\cdot(\hat{\mathbf{S}}^{\mathrm{t}}\otimes\hat{1}^{\mathrm{s}})+U^{\mathrm{t}}\hat{\sigma}_0\cdot\hat{1}^{\mathrm{ts}}\right)\left(\frac{1}{2}\hat{\boldsymbol{\sigma}}\cdot(\hat{1}^{\mathrm{t}}\otimes\hat{\mathbf{S}}^{\mathrm{s}})+U^{\mathrm{s}}\hat{\sigma}_0\cdot\hat{1}^{\mathrm{ts}}\right)\\
&+\left(\frac{1}{2}\hat{\boldsymbol{\sigma}}\cdot(\hat{1}^{\mathrm{t}}\otimes\hat{\mathbf{S}}^{\mathrm{s}})+U^{\mathrm{s}}\hat{\sigma}_0\cdot\hat{1}^{\mathrm{ts}}\right)\left(\frac{1}{2}\hat{\boldsymbol{\sigma}}\cdot(\hat{\mathbf{S}}^{\mathrm{t}}\otimes\hat{1}^{\mathrm{s}})+U^{\mathrm{t}}\hat{\sigma}_0\cdot\hat{1}^{\mathrm{ts}}\right)\\
=\;&\frac{1}{4}\sum_{\substack{i=\\x,y,z}}\sum_{\substack{j=\\x,y,z}}\left[\hat{\sigma}_i(\hat{S}_i^{\mathrm{t}}\otimes\hat{1}^{\mathrm{s}})\hat{\sigma}_j(\hat{1}^{\mathrm{t}}\otimes\hat{S}_j^{\mathrm{s}})+\hat{\sigma}_j(\hat{S}_i^{\mathrm{t}}\otimes\hat{1}^{\mathrm{s}})\hat{\sigma}_i(\hat{1}^{\mathrm{t}}\otimes\hat{S}_j^{\mathrm{s}})\right]\\
&+U^{\mathrm{t}}\sum_{\substack{i=\\x,y,z}}\hat{\sigma}_i(\hat{1}^{\mathrm{t}}\otimes\hat{S}_i^{\mathrm{s}})+U^{\mathrm{s}}\sum_{\substack{i=\\x,y,z}}\hat{\sigma}_i(\hat{S}_i^{\mathrm{t}}\otimes\hat{1}^{\mathrm{s}})+... \qquad \text{(S20)}\\
=\;&\sum_{\substack{i=\\x,y,z}}\left[\frac{1}{2}\hat{\sigma}_0(\hat{S}_i^{\mathrm{t}}\otimes\hat{S}_i^{\mathrm{s}})+U^{\mathrm{t}}\hat{\sigma}_i(\hat{1}^{\mathrm{t}}\otimes\hat{S}_i^{\mathrm{s}})+U^{\mathrm{s}}\hat{\sigma}_i(\hat{S}_i^{\mathrm{t}}\otimes\hat{1}^{\mathrm{s}})\right]+..., \qquad \text{(S21)}
\end{aligned}
$$

where the ... denote the neglected terms of order $U^{\mathrm{t}}U^{\mathrm{s}}$.

The last simplification which reduces the double summation in S20 to a single one in S21 originates from the fundamental commutator relations of the electron's orthonormal angular momentum operators: $\hat{\sigma}_i\hat{\sigma}_j+\hat{\sigma}_j\hat{\sigma}_i=[\hat{\sigma}_i,\hat{\sigma}_j]_+\equiv 2\delta_{i,j}\hat{\sigma}_0$, which leads directly to the transition matrix elements as shown in equation 4 of the main paper.

In summary, the spectrum of a system with two active spins on tip and sample contains contributions of each individual spin weighted by the Coulomb scattering rate of the respectively other spin plus an additional term in which angular spin momentum is exchanged only between both spin systems leaving the tunneling electron's spin momentum unchanged.